A Continuum Model for Carbon Nanotube-Infused Polyimides

Heather Wilson[1], Sumanth Banda[2], Ralph C. Smith[3], and Zoubeida Ounaies[4]

Department of Mathematics[1,3]
Center for Research in Scientific Computation
North Carolina State University
Raleigh, NC 27695

Aerospace Engineering Department[2,4]
Texas A&M
College Station, TX 77843

Abstract

Polyimides are presently being investigated for a wide range of aeronautic, aerospace and industrial applications due to the fact that they have good thermal and chemical resistance yet are flexible. Within the realm of aerospace applications, polyimides can be employed for deployment, positioning, and vibration attenuation of large structures including thin-film membrane mirrors and gossamer antennas. The inclusion of single wall carbon nanotubes raises the conductivity levels to permit electric discharge. Additionally, they augment the electromechanical coupling properties of piezoelectric polyimides to provide them with actuator capabilities. We present a temperature-dependent material model based on elasticity theory which characterizes stiffness through the material as a function of varying concentrations of single wall nanotubes (SWNT). We begin by investigating the temperature affects on the polyimide. We then discuss the effects of SWNT volume concentration on the composite storage modulus. The composite model takes into account the alignment, interphase, and geometry of the SWNTs.

Keywords: Carbon nanotubes, polyimide, polymer matrix composites, mechanical properties

1. Introduction

Polyimides are a class of polymers that are thermally and chemically stable and radiation resistant. In addition to their stability, polyimides possess a relatively large elastic modulus and are flexible. Their stability and stiffness make them good candidates for use in space applications. However, due to their insulating nature, static charge buildup can deteriorate the structure. This charge buildup can be eliminated by embedding single wall nanotubes (SWNTs) into the polyimide. SWNTs are excellent conductors and have a high elastic modulus. Thus, embedding the SWNTs into the polyimide not only introduces conductivity but also increases the stiffness of the composite. SWNTs can also be added to create an active structure from inactive polyimides [3, 13].

Nanotechology is being investigated for use in constructing large ultra-lightweight (gossamer) spacecraft. Since the gossamer spacecraft is folded and packed into the shuttle prior to launch, the materials need to withstand this process. The nanotube-infused polyimides are flexible enough to withstand the packaging process and strong enough to withstand the harsh space environment. Specific applications of the gossamer spacecraft include thin-film membrane mirrors and gossamer antennas.

Nanotube composites have been modeled in the past using a variety of techniques. However, much of the previous work focused on modeling the elastic modulus at a set temperature. Since temperatures widely vary in space, a temperature-dependent model is required for the elastic modulus. There are a few approaches

[1]Email: hlwilson@ncsu.edu
[2]Email: sumanth@tamu.edu
[3]Email: rsmith@eos.ncsu.edu, Telephone: (919) 515-7552
[4]Email: zounaies@tamu.edu,

taken when modeling nanotube composites. The first focuses on the molecular level. Molecular models use simulations to determine local interactions among atoms or chemical reactions between the matrix and nanotubes [5, 9, 10, 11]. Molecular models are limited to very small systems due to the high computational cost. The second is continuum modeling which considers overall deformations. Continuum models include the Mori-Tanaka model, rule of mixtures, and the Halpin Tsai model [4, 7, 8]. We will expand on previous work reported in [4, 16].

In this work, we present a temperature-dependent continuum material model, based on phenomenological elasticity theory, which characterizes stiffness through the material as a function of varying concentrations of nano-inclusions. Attributes of the model are illustrated through comparison with experimental data for the polyimide (β-CN)-APB/ODPA.

In Section 2, a temperature-dependent model for the polyimide (β-CN)-APB/ODPA is derived. The composite model for the polyimide infused with SWNTs is developed in Section 3. In this section, model considerations such as alignment, interphase, and geometry are discussed. Finally, the composite model is compared to the data and results are discussed.

2. Temperature-Dependent Polyimide Model

To describe the composite material, we must first understand how temperature affects the polyimide. At lower temperatures, the polyimide is in a glassy or frozen state. The polymer chains are locked together resulting in a high storage modulus, on the order of gigapascals. As the material is heated, secondary bonds weaken and side groups and chain segments become mobile releasing energy and therefore drastically reducing the storage modulus. The region in which this occurs is termed the glass transition region. Although it is actually a range of temperatures in which the change occurs, it is typically reported as one temperature referred to as the glass transition temperature T_g. The glass transition temperature can be determined through a variety of methods such as Differential Scanning Calorimetry and Thermal-Mechanical Analysis [1]. In this investigation, the glass transition temperature is taken to be the temperature at which the loss tangent peaks [15]. The storage and loss modulus, E' and E'', and loss tangent, $\tan\delta$, for the polyimide are shown in Figure 1.

The three elements in Figure 2 represent the state of the polyimide before, during, and after the glass transition region. We derive an expression for the storage modulus of the polyimide both before and after the glass transition region. The storage modulus of the polyimide in the glassy region is referred to as the frozen storage modulus and the storage modulus for the polyimide in the rubbery region is referred to as the active storage modulus. The transition region is described with a function, termed the frozen fraction, that is related to the distribution of the loss tangent [16].

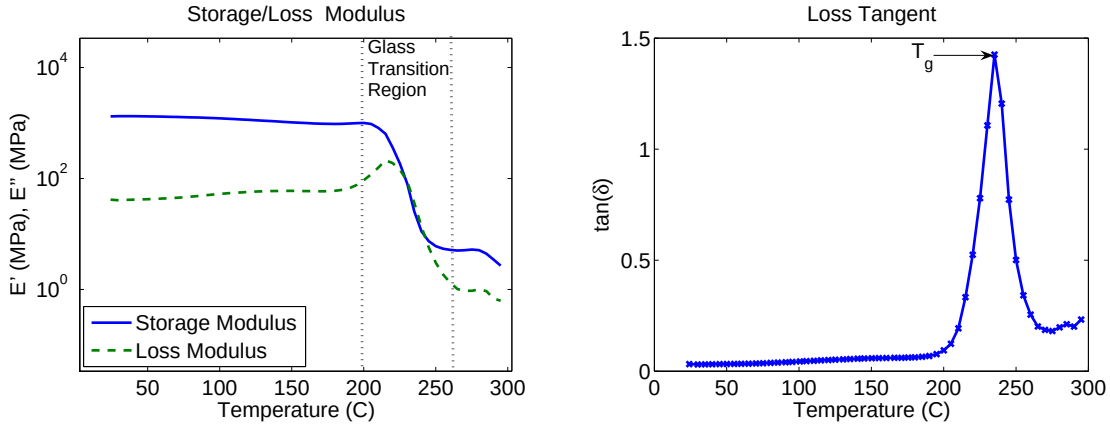

(a) E', E'' (b) $\tan\delta$

Figure 1: (a) Storage modulus E', loss modulus E'' and (b) loss tangent $\tan\delta$ for the temperature range under consideration.

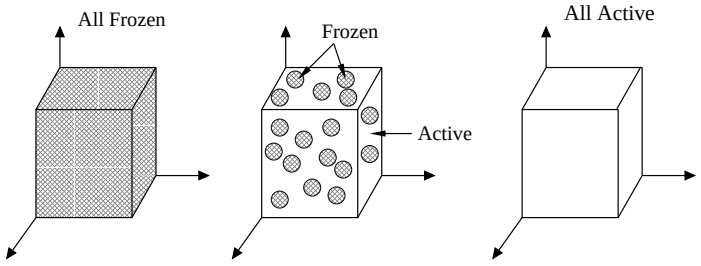

(a) $T \ll T_g$ (b) Glass Transition Region (c) $T \gg T_g$

Figure 2: Polymer phase (a) below the glass transition region, (b) in the glass transition region, and (c) above the glass transition region.

If a stress σ is applied at temperature T, the stress-strain relation can be formulated as

$$\sigma(T) = \frac{E'(T)\epsilon(T)}{\cos\delta(T)}$$

where $\epsilon(T)$ denotes the temperature-dependent strain. Now consider the active and frozen phases having the same stress applied without varying temperature. The active material experiences a strain $\epsilon^a(T)$ and the frozen material experiences a strain $\epsilon^f(T)$. Using the rule of mixtures to describe the strain exhibited by the bulk material, we obtain

$$\sigma(T) = \frac{E'(T)}{\cos\delta(T)}\left[\phi^f(T)\epsilon^f(T) + (1-\phi^f(T))\epsilon^a(T)\right]$$

where $\phi^f(T)$ is the volume fraction of the frozen phase present in the bulk material.

Formulating the active and frozen strain as a function of its modulus and applied stress, we obtain the relation

$$\sigma(T) = \frac{E'(T)}{\cos\delta(T)}\left[\phi^f(T)\frac{\sigma(T)\cos\delta(T)}{E^f(T)} + (1-\phi^f(T))\frac{\sigma(T)\cos\delta(T)}{E^a(T)}\right]$$

for the bulk material where $E^a(T)$ and $E^f(T)$ are the storage moduli of the active and frozen phases. The storage modulus of the bulk material is

$$E'(T) = \frac{1}{\dfrac{\phi^f(T)}{E^f(T)} + \dfrac{1-\phi^f(T)}{E^a(T)}}.$$

2.1 Frozen and Active Storage Modulus

At temperatures below the glass transition region, little damping is observed in the data ($\delta \approx 0$). This is due to the fact that the polymer chains are still tightly packed and little energy is dissipated. For small phase lags, the storage modulus can be approximated by the elastic modulus, thus yielding the relations

$$\begin{aligned} E'(T) &= \frac{\sigma(T)}{\epsilon(T)}\cos\delta(T) \approx \frac{\sigma(T)}{\epsilon(T)} = E(T) \\ E''(T) &= \frac{\sigma(T)}{\epsilon(T)}\sin\delta(T) \approx 0. \end{aligned}$$

Since ($\delta \approx 0$), the elastic modulus is approximated using Hooke's law, $\sigma = E\epsilon$. Therefore, the frozen storage modulus is

$$(E^f)'(T) = E(T) = \frac{\sigma(T)}{\epsilon(T)}.$$

In the experiments performed in this investigation, a constant strain of 0.28% was applied.

Above the glass transition region, the polyimide is in a rubbery state. In this rubbery region, linear polymer chain motion is restricted by chain entanglements. The storage modulus is increased with an increased number chain entanglements. Energy relations are used to derive a model for the storage modulus above the glass transition region [17]. In rubbery materials, the deformation is due to entropy. For an incompressible material with small strains, the storage modulus is given by

$$E^a(T) = 3NkT$$

where N is a measure of chain entanglements and k is Boltzmann's constant. The measure of chain entanglements is determined by solving for N at $T = 275°$ C, which gives $N = 2.3086 \times 10^{26}$. The models for the frozen and active storage modulus are compared with the data in Figure 3. Notice that the storage modulus begins to decrease around $T = 280°$ C. At this point the material has begun to transition into viscous liquid [2] so we do not expect the present model to predict this decrease.

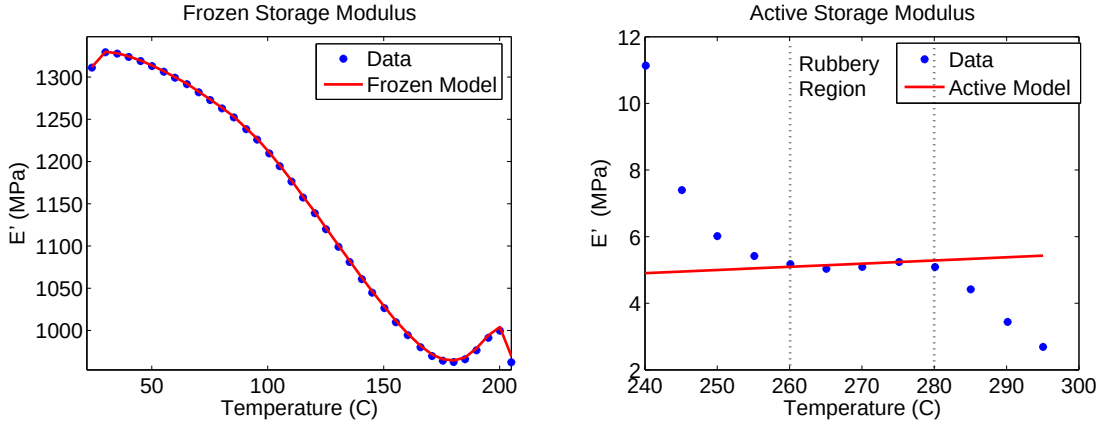

(a) Frozen Modulus (b) Active Modulus

Figure 3: Model for (a) the frozen storage modulus and (b) the active storage modulus of the polyimide.

2.2 Frozen Fraction

Now that we have derived models for the frozen and active states, we need to describe the transition between the two states. As the temperature is increased and enters the glass transition region, both active and frozen states occur. The frozen fraction quantifies the volume fraction of frozen phase material at each temperature.

In the transition region, chain segments and side group become more mobile and secondary bonds weaken dissipating energy. This dissipated energy can be related to the loss tangent. The temperature range which the loss tangent peak spans is roughly equal to the temperature range of the glass transition region. We begin by modeling the loss tangent with a continuous probability density function with normal distribution,

$$\varphi(T) = \frac{1}{\sigma\sqrt{2\pi}} \exp\left(-\frac{(T-\mu)^2}{2\sigma^2}\right) \tag{1}$$

where μ and σ^2 are the mean and variance of the loss tangent peak with respect to temperature. The integration constant $\frac{1}{\sigma\sqrt{2\pi}}$ is replaced by a factor K which is equal to the loss tangent value at T_g.

We let the frozen fraction at T_0 be the percentage of the area under the distribution for $T > T_0$,

$$\phi_0(T) = \frac{\int_T^\infty \varphi(\theta)d\theta}{\int_{\mathbb{R}} \varphi(\theta)d\theta}.$$

From (1) it follows that

$$\begin{aligned}\int_T^\infty \varphi(\theta)d\theta &= \int_T^\infty K\exp(-c(\theta-T_g)^2)d\theta \\ &= \frac{K\sqrt{\pi}}{2\sqrt{c}}\frac{2}{\sqrt{\pi}}\int_{\sqrt{c}(T-T_g)}^\infty \exp(-u^2)du \\ &= \frac{K\sqrt{\pi}}{2\sqrt{c}}[1-\mathrm{erf}(\sqrt{c}(T-T_g))]\end{aligned}$$

and

$$\int_{\mathbb{R}} \varphi(\theta)d\theta = \frac{K\sqrt{\pi}}{\sqrt{c}}$$

where $c = 1/2\sigma^2$. Therefore, the frozen fraction is quantified by the relation

$$\phi_0(T) = \frac{1-\mathrm{erf}(\sqrt{c}(T-T_g))}{2}.$$

The frozen fraction is used to eliminate the bias β_f and β_a in the frozen and active states. The loss tangent with the bias removed is

$$\tan\delta_{adj}(T) = \tan\delta(T) - \beta_f\phi_0(T) - \beta_a(1-\phi_0(T))$$

where β_f and β_a are 0.0305 and 0.1807, respectively, for the data under consideration.

Since a single distribution is not adequate to approximate the loss tangent, a 2 term Galerkin expansion

$$\tan\delta(T) \approx \varphi(T) = \sum_{i=1}^{2} w_i\varphi_i(T),$$

is used so that

$$\varphi(T) = K_1\exp(-c_1(T-T_{g1})^2) + K_2\exp(-c_2(T-T_{g2})^2). \tag{2}$$

The first term approximates the peak of the loss tangent and the second term approximates the dissipation away from the peak [16]. The optimal values obtained through a least squares fit to the data are

$$\begin{array}{lll} K_1 = 0.7678, & \sigma_1^2 = 1/(2c_1) = 166.6667, & T_{g1} = 232.5181 \\ K_2 = 0.5715, & \sigma_2^2 = 1/(2c_2) = 26.4550, & T_{g2} = 236.2570. \end{array}$$

Figure 4 shows the results of the model for the loss tangent. The term from (2) with the lower standard deviation is taken as the probability distribution

$$\varphi(T) = K_2\exp\left(-c_2(T-T_{g2})^2\right).$$

Therefore, we define the temperature-dependent frozen fraction as

$$\phi(T) = \frac{1-\mathrm{erf}\left(\sqrt{c_2}(T-T_{g2})\right)}{2}.$$

Now that we have expressions for the frozen and active modulus and the frozen fraction, we can complete the model for the storage modulus of the polyimide. The model is compared with the data in Figure 5. The corresponding model for the storage modulus of the polyimide is

$$E'(T) = \frac{1}{\dfrac{\phi^f(T)}{E^f(T)} + \dfrac{1-\phi^f(T)}{3NkT}} \tag{3}$$

where

$$\phi^f(T) = \frac{1-\mathrm{erf}[\sqrt{0.0189}(T-236.2570)]}{2}.$$

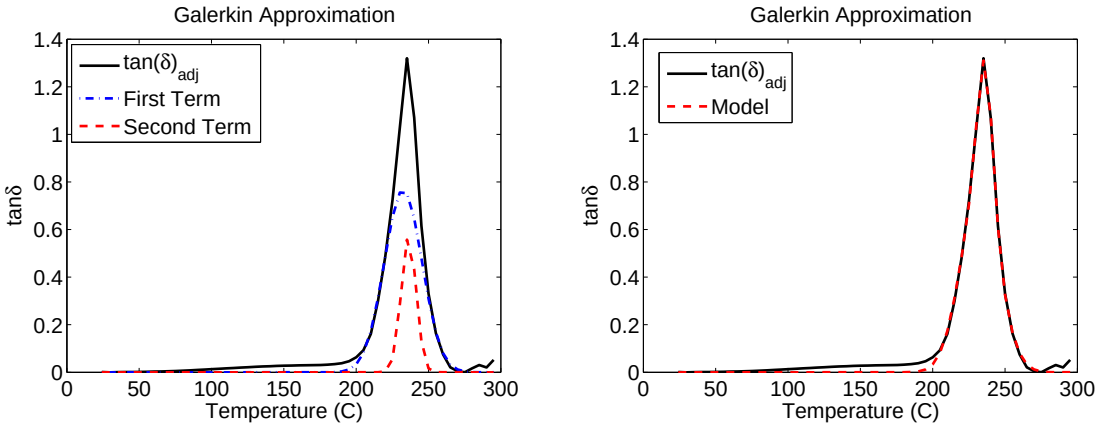

(a) Peak and dissipation terms

(b) Loss tangent model

Figure 4: Galerkin approximation for loss tangent of the polyimide. (a) Individual terms in the Galerkin expansion. (b) Sum of the terms in the Galerkin expansion.

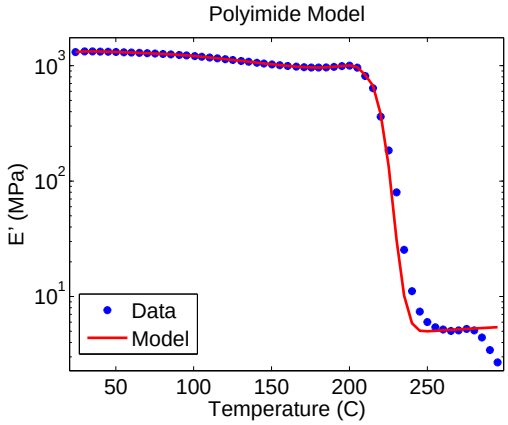

Figure 5: Temperature-dependent model (3) and experimental data for the storage modulus of the polyimide.

3. Composite Model

Experiments were performed for SWNT concentrations of 0.035 vol%, 0.05 vol%, 0.075 vol%, 0.1 vol%, 1 vol% and 2 vol%, yielding the storage modulus E' shown in Figure 6. The 0.1% data set should be considered with care since the storage modulus is much lower than expected. It should also be noted that the 0.075% appears to have an outlying glass transition temperature as shown in Figure 7. All the data sets have a standard deviation of approximately 10°C. At concentrations above 0.1%, it is noticed that the nanotubes begin to bundle which may effect the storage modulus.

We applied the previously derived model to the composite data sets, but no correlation was found between the calculated parameters N, T_{g2}, and c_2 and the volume fraction. Therefore, (3) is used to model temperature-dependent storage modulus of the polyimide E_m in the following composite model.

3.1 Halpin Tsai Model

As stated previously, incorporation of SWNTs into the polyimide increases the storage modulus at each temperature, but seems to have little effect on the temperature-dependence of the composite storage modulus. The temperature-dependence is introduced via the model for the storage modulus of the polyimide. The storage modulus of the polyimide E_m is replaced with (3).

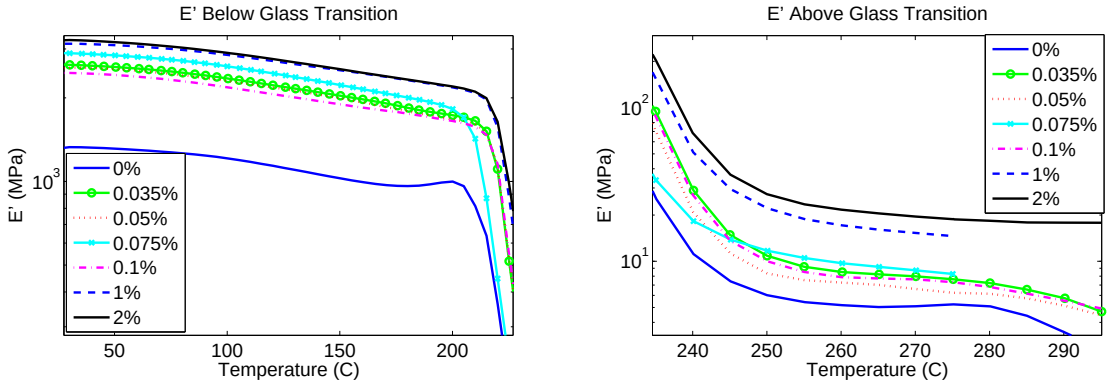

(a) Frozen Region (b) Active Region

Figure 6: Storage modulus E' for temperatures (a) below and (b) above the glass transition region.

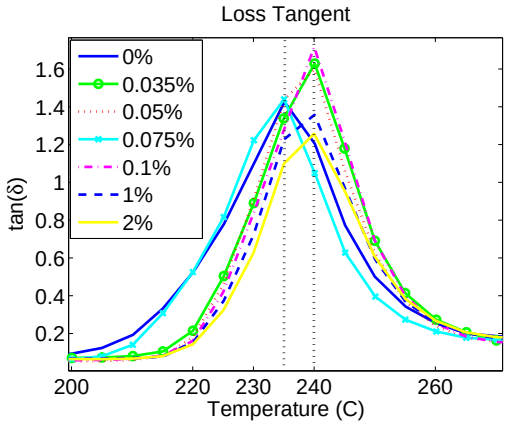

Figure 7: Loss tangent for all data sets. The glass transition temperature for 0.075% is the same as for the polyimide. All other data sets are 5°C higher.

The Halpin Tsai composite model [6] predicts the increase in storage modulus with increasing SWNT concentrations for oriented inclusions. The longitudinal and transverse storage modulus can be calculated as

$$E_c' = \left(\frac{1+\zeta\eta V_f}{1-\eta V_f}\right) E_m$$

where

$$\eta = \left(\frac{E_f}{E_m} - 1\right) / \left(\frac{E_f}{E_m} + \zeta\right).$$

Here ζ is a shape parameter that depends on the filler geometry and loading direction, V_f is the volume fraction of the inclusion, and E_f is the storage modulus of the inclusion. The storage modulus of a SWNT is approximately 1 TPa. For transverse loading $\zeta = 2$, and for longitudinal loading $\zeta = L_f/r_f$. The length and radius of the nanotubes used in the experiment are $L_f = 1\mu$m and $r_f = 0.4$nm.

3.2 2D Random Fiber Orientation

The Halpin Tsai equations are designed for inclusions that all have the same orientation. Since the SWNTs are randomly oriented, we must make modifications to the Halpin Tsai model. As illustrated Figure 8, we consider a single fiber rotated at an angle ϕ from the 1-axis with an applied strain ϵ_{11}.

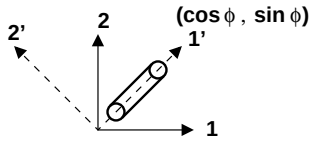

Figure 8: Fiber rotated ϕ from the 1-axis.

The translation of ϵ_{11} onto the 1'2' axis yields the strains

$$\epsilon'_{11} = \epsilon_{11}\cos^2\phi, \quad \epsilon'_{12} = \epsilon'_{21} = -\epsilon_{11}\sin\phi\cos\phi, \quad \epsilon'_{22} = \epsilon_{11}\sin^2\phi. \tag{4}$$

Using Hooke's law and (4), the corresponding stresses in the 1'2' plane are

$$\frac{\sigma'_{11}}{\epsilon_{11}} = E'_{11}\cos^2\phi, \quad \frac{\sigma'_{12}}{\epsilon_{11}} = \frac{\sigma'_{21}}{\epsilon_{11}} = -E'_{12}\sin\phi\cos\phi, \quad \frac{\sigma'_{22}}{\epsilon_{11}} = E'_{22}\sin^2\phi. \tag{5}$$

The stress in the 11 direction is

$$\sigma_{11} = \sigma'_{11}\cos^2\phi - 2\sigma'_{12}\sin\phi\cos\phi + \sigma'_{22}\sin^2\phi. \tag{6}$$

Substituting (5) into (6), and solving for the stiffness in the 11 direction yields

$$E_{11} = \frac{\sigma_{11}}{\epsilon_{11}} = E'_{11}\cos^4\phi + 2E'_{12}\sin^2\phi\cos^2\phi + E'_{22}\sin^4\phi.$$

To determine the stiffness in the 11 direction for a random orientation we integrate

$$E_{11}|_{random} = \frac{\sigma_{11}}{\epsilon_{11}}|_{random} = \frac{1}{\pi}\int_0^\pi (E'_{11}\cos^4\phi + 2E'_{12}\sin^2\phi\cos^2\phi + E'_{22}\sin^4\phi)d\phi.$$

Therefore the stiffness in the 11 direction for fibers randomly orientated in 2D is

$$E_{11} = \frac{3}{8}E_L + \frac{3}{8}E_T + \frac{2}{8}E'_{12}$$

where

$$E'_{12} = 2\mu_{12}(1+\nu_{12}).$$

The longitudinal shear modulus, μ_{12} can be calculated using the Halpin Tsai relation where $\zeta = 1$,

$$\mu_{12} = \frac{1+\zeta\eta V_f}{1-\eta V_f} \quad \text{where} \quad \eta = \frac{\mu_f/\mu_m - 1}{\mu_f/\mu_m + \zeta}.$$

The Poisson's ratio for small volume fractions is estimated to be

$$\nu_{12} = V_f\nu_f + (1-V_f)\nu_m$$

where 0.34 and 0.19 are the Poisson's ratios for the polyimide and SWNT [14]. The longitudinal and transverse stiffness are calculated using the Halpin Tsai model with $\zeta = L_f/r_f$ and $\zeta = 2$.

3.3 Interphase Region

An interphase region is thought to form around the SWNTs, which would increase the expected storage modulus for the composite. In previous work reported in [4], it is observed that incorporation of an interphase region into the Halpin Tsai model improves predictions of the composite storage modulus. To describe this phenomenon, we assume a cylindrical interphase with thickness $t_o = r_f$ forms around the SWNT. The stiffness of the interphase is taken to be the average of the polyimide and SWNT stiffness. Figure 9 depicts the geometry under consideration.

It should be noted that the volume fraction of the inclusion phase is altered with the incorporation of the interphase. The inclusion phase should include the volume occupied by both the SWNT and the interphase. The volume fraction of the interphase can be formulated as

$$V_{inter} = V_f \frac{(t_0 + r_f)^2 - r_f^2}{r_f^2}$$

where V_f is the volume fraction of the SWNT and t_0 is the thickness of the interphase wall. The volume fraction of the interphase/SWNT is

$$V^* = V_f \frac{(t_0 + r_f)^2}{r_f^2}.$$

It should also be noted that ζ for the longitudinal modulus will decrease since the thickness of the inclusion has increased, $\zeta = l_f/(r_f + t_o)$.

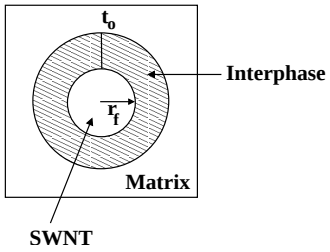

Figure 9: Geometry of SWNT surrounded by interphase region in a polyimide matrix.

3.4 SWNT geometry

Typically a SWNT is treated a a solid cylinder when it is in fact a hollow cylinder with shell thickness 66 pm [12]. We consider both geometries. For the shell geometry we consider two cases. The first case is a hollow shell with interphase forming on the outside of the shell and matrix material in the core of the shell. The second case is a hollow shell with outer interphase and core filled with interphase material.

3.5 Modified Halpin Tsai Model

We are now ready to incorporate the randomly oriented fibers, the interphase, and the SWNT geometry into the Halpin Tsai model. The resulting interphase model is plotted for the 0.035 vol%, 0.075 vol%, 1 vol%, and 2 vol% data sets in Figures 10 and 11. When considering a SWNT with shell geometry we represent the 3 cases as *Shell*, $Shell_{IM}$, and $Shell_{II}$. *Shell* refers to a SWNT with shell geometry without an interphase, $Shell_{IM}$ refers to the case with an interphase forming on the outer surface of the SWNT, and $Shell_{II}$ refers to the case with an interphase forming on both the outer and inner surface.

The Halpin Tsai model under-predicts below the glass transition region for the low volume fractions. As the volume fraction is increased, the predicted storage modulus also increases. At higher concentrations, it can be noticed that the model with a shell geometry gives a fair prediction of the storage modulus and the other model greatly over-predict. This over-prediction is most likely due to the fact that nanotubes begin to bundle at higher concentrations.

4. Concluding remarks

A temperature-dependent model for the storage modulus of the polyimide (β-CN)-APB/ODPA was derived. The temperature-dependent model was then incorporated in a modified Halpin Tsai model to predict the effects increasing SWNT concentrations have on the composite storage modulus. The random alignment, interphase, and SWNT geometry were taken into consideration when modifying the Halpin Tsai model. The composite model under-predicts at temperatures below the glass transition region for lower concentrations and over-predicts for higher concentrations. A viscoelastic model will likely be needed to more accurately describe the glass transition region.

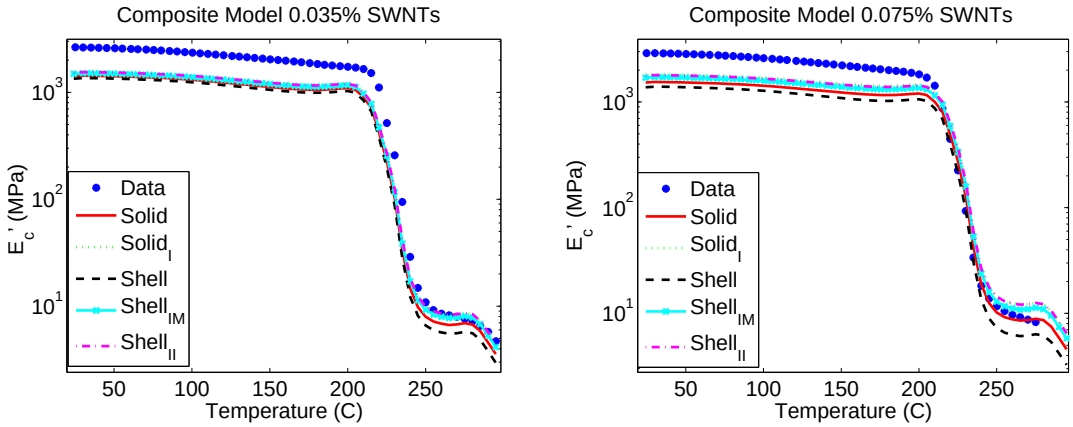

Figure 10: Modified Halpin Tsai model that incorporates interphase and randomly aligned fibers for low volume fractions.

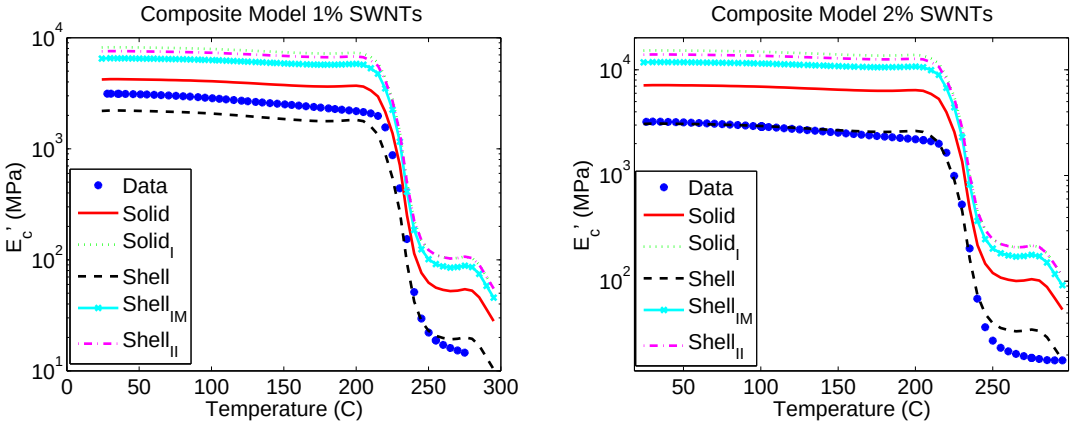

Figure 11: Modified Halpin Tsai model that incorporates interphase and randomly aligned fibers for high volume fractions.

Acknowledgements

The research of HW was supported by the Science, Mathematics and Research for Transformation (SMART) fellowship which is funded by the Department of Defense. The research of RCS was supported in part by the Air Force Office of Scientific Research through the grants AFOSR-FA9550-04-1-0203 and AFOSR-FA9550-08-1-0348. The research of SB and ZO was supported in part by the NSF through the grants NSF CMMI 0645185 and NSF CMMI 0514265.

References

[1] "Arlon application notes, measuring and understanding Tg (glass transition temperature)," www.arlon-med.com/Measuring%20and%20Understanding%20Tg.pdf.

[2] Aklonis, J. and MacKnight, W., *An Introduction to Polymer Viscoelasticity*, John Wiley and Sons, Ch.3, 1983.

[3] Deshmukh, S., Call, C., Ounaies, Z., Park, C., and Harrison, J., "Effect of single walled carbon nanotubes (SWNTs) on the electromechanical response of a polyimide nanocomposite," *Proc. SPIE*, **6168**, pp. 61680Y-1-61680Y-10, 2006.

[4] Eitan, A., Fisher, F.T., Andrews, R., Brinson, L.C., and Schadler, L.S., "Reinforcement mechanisms in MWCNT-filled polycarbonate," *Composites Science and Technology*, **66**, pp. 1162-1173, 2006.

[5] Frankland, S., Harik, V., Odegard, G., Brenner, D., and Gates, T., "The stress-strain behavior of polymer-nanotube composites from molecular dynamics simulation," *Composites Science and Technology*, **63**, pp. 1655-1661, 2003.

[6] Halpin, J.C. and Kardos, J.L., "The Halpin-Tsai equation: A review," *Polymer Engineering and Science*, **16**(5), pp. 344-352, May 1976.

[7] Hashin and Rosen, "The elastic moduli of fiber reinforced materials," *Journal of Applied Mechanics*, **31**, pp. 223-232, June 1964.

[8] Jones, R.M., *Mechanics of Composite Materials*, Hemisphere Publishing Corp, NY, 1975.

[9] Liu, Y.J. and Chen, X.L., "Continuum models of carbon nanotube-based composites using the boundary element method," *Electronic Journal of Boundary Elements*, **1**(2), pp. 316-335, 2003.

[10] Lordi, V. and Yao, N., "Molecular mechanics of binding in carbon-nanotube-polymer composites," *Journal of Material Research*, **15**(12), pp. 2770-2779, 2000.

[11] Meo, M. and Rossi, M., "Prediction of Young's modulus of single wall carbon nanotubes by molecular-mechanics based finite element modelling," *Composites Science and Technology*, **66**, pp. 1597-1605, 2006.

[12] Odegard, G., Gates, T., Nicholson, L., and Wise, K., "Equivalent-continuum modeling of nano-structured materials," *Composites Science and Technology*, **62**, pp. 1869-1880, 2002.

[13] Ounaies, Z., Park, C., Harrison, J., et al., "Evidence of piezoelectricity in SWNT-polyimide and SWNT-PZT-polyimide composites," *Journal of Thermoplastic Composite Materials*, **21**(5), pp. 393-409, 2008.

[14] Park, C., Kang,J.H., Harrison, J.S., Costen, R.C., and Lowther, S.E., "Actuating single wall carbon nanotube-polymer composites: intrinsic unimorphs," *Advanced Materials*, **20**(11), pp. 2074-2079, 2008.

[15] Shaffer, M., and Windle, A., "Fabrication and characterization of carbon nanotube/poly(vinyl alcohol) composites," *Advanced Materials*, **11**(11), pp. 937-941, 1999.

[16] Siskind, R.D., *Model Development for Shape Memory Polymers*, *Ph.D Thesis*, Department of Applied Mathematics, North Carolina State University, 2008.

[17] Ward, I. and Hadley, D., *An Introduction to the Mechanical Properties of Solid Polymers*, John Wiley and Sons, 1993.